Biochimica et Biophysica Acta 1838 (2014) 814–821

Contents lists available at ScienceDirect

Biochimica et Biophysica Acta

journal homepage: www.elsevier.com/locate/bbamem

Electroporation of heterogeneous lipid membranes

Ramon Reigada *

Departament de Química Física and Institut de Química Teòrica i Computacional (IQTCUB), Universitat de Barcelona, Barcelona, Spain

ARTICLE INFO

Article history:
Received 12 May 2013
Received in revised form 25 September 2013
Accepted 3 October 2013
Available online 18 October 2013

Keywords:
Electroporation
Molecular dynamics
Numerical simulations
Structured lipid membrane
Liquid-ordered phase
Liquid-disordered phase

ABSTRACT

Electroporation is the basis for the transfection of genetic material and for drug delivery to cells, including electrochemotherapy for cancer. By means of molecular dynamics many aspects of membrane electroporation have been unveiled at the molecular detail in simple, homogeneous, lipid bilayers. However, the correspondence of these findings \with the process happening in cell membranes requires, at least, the consideration of laterally structured membranes. Here, I present a systematic molecular dynamics study of bilayers composed of different liquid-ordered and liquid-disordered lipid phases subjected to a transversal electric field. The simulations reveal two significant results. First, the electric field mainly affects the properties of the disordered phases, so that electroporation takes place in these membrane regions. Second, the smaller the disordered domains are, the faster they become electroporated. These findings may have a relevant significance in the experimental application of cell electroporation *in vivo* since it implies that electro-induced and pore-mediated transport processes occur in particularly small disordered domains of the plasma membrane, thus locally affecting only specific regions of the cell.

1. Introduction

Reversible pores in cell membranes can be induced by the application of an electric field. This technique is referred as electropermeabilization or electroporation [1], and has been used in numerous applications in biotechnology and medicine. It is a common technique for introducing genetic material in cells [2], and for delivering drugs across the cell membrane [3]. The latter application has resulted in a tool to battle cancer, the electrochemotherapy [4,5], based on the electroformation of reversible pores in the cell membrane, allowing the delivery of non-permeant drugs inside tumor cells and locally enhancing their cytotoxic effects.

Atomistic molecular dynamics (MD) simulations have been adopted as a powerful method to study membrane pore formation when a transverse electric field is applied [6]. Following this approach, several works have been devoted to the numerical investigation of electroporation in single-component bilayers, the molecular mechanism of this phenomenon has been unveiled, at least for simple systems [7–9], and the different stages of pore formation have been characterized [10]. Recently, MD numerical simulations have even reproduced the transfection of a siRNA double-strand following the latter mentioned pore-mediated mechanism [11].

Despite its doubtless utility, MD studies performed so far have a major drawback. Real biological membranes are not homogeneous bilayers but lateral heterogeneous media with a complex nanoscale lipidic organization [12]. There is a general consensus that cell membranes are laterally structured in fluid regions with different phasic behavior and lipid composition. As a first approximation, this view can be simplified as the coexistence of liquid-ordered (*lo*) phases containing saturated lipids and cholesterol, and liquid-disordered (*ld*) phases rich in unsaturated lipids and low contents of cholesterol [13,14]. Such organization is often conceptualized in terms of nanoscale aggregates of saturated lipids and cholesterol, referred as lipid rafts [15], surrounded by a *ld* lipid phase. Therefore, any correlation between results from MD simulations of electroporation in lipid bilayers and the electroporation phenomenon in biological membranes should consider, at least at a simple level, the organization in *lo*/*ld* regions. This step has been done here by performing a collection of systematic atomistic MD simulations of laterally structured lipid membranes under the influence of a transversal electric field. The role of the phasic characteristics and size of membrane domains is analyzed with respect to their ability to become electroporated.

2. Methods

Atomistic MD simulations of phospholipid bilayer systems composed of dioleoylphosphatidylcholine (DOPC), distearoylphosphatidylcholine (DSPC) and cholesterol (Chol) have been carried out. Simulations were performed using the GROMACS software package [16]. For the phospholipid molecules, the standard united-atom force-field parameters developed by Berger et al. [17] were used together with the appropriate

Abbreviations: MD, Molecular dynamics; *lo*, Liquid-ordered; *ld*, Liquid-disordered; Chol, Cholesterol; DOPC, Dioleoylphosphatidylcholine; DSPC, Distearoylphosphatidylcholine

* c/ Marti i Franques 1, Planta 4, 08028 Barcelona, Spain. Tel.: +34 934039290.
E-mail address: reigada@ub.edu.

0005-2736/$ – see front matter © 2013 Elsevier B.V. All rights reserved.
http://dx.doi.org/10.1016/j.bbamem.2013.10.008

correction for the double-bond description in DOPC [18]. The force field parameters of Holtje et al. [19] were adapted for Chol, and the simple point charge model was employed for water. LINCS and SETTLE algorithms were used to preserve bond lengths in lipid and water molecules, respectively. A single 1.0 nm cut-off distance was used for Lennard–Jones interactions, and electrostatic interactions were handled using the particle-mesh Ewald method with a real space cut-off of 1.0 nm. Periodic boundary conditions were used in all three directions, and the time step was set to 2 fs. Simulations were carried out in the NpT ensemble at $p = 1$ atm and $T = 310$ K. The pressure coupling was applied separately in the bilayer plane (x,y) and the perpendicular direction (z). This simulation protocol has been successfully applied in previous MD simulations [20], and the obtained values for structural membrane properties (in the absence of an external electric field) such as the area per molecule, the membrane thickness, and the scattering form factors are consistent with experimental data for DOPC and DOPC/Chol bilayers (see Ref. [20]).

The simulated bilayers consist in different combinations of *ld* and *lo* phases, the former exclusively composed by the unsaturated lipid DOPC, and the latter represented by a mixture of the fully saturated lipid DSPC and 20%mol Chol. A first set of simulations is performed for bilayers composed of a central *lo* patch surrounded by a *ld* phase, mimicking the structure of a lipid raft nanodomain [15]. The initial structure of this membrane system was generated from an equilibrated DSPC/Chol bilayer where all Chol and DSPC molecules placed further than a given distance from the center of the (x,y) simulation plane were removed or changed to DOPC, respectively. The mentioned distance was chosen so that the final system contained 256 DOPC, 256 DSPC and 64 Chol molecules, evenly distributed in the two leaflets. A circular patch of DSPC/20%Chol surrounded by DOPC was obtained as a starting configuration for the raft-like membrane system. A second set of simulations corresponds to the inverse configuration: a central *ld* domain (256 DOPC molecules, *ld*_256 domain) surrounded by a *lo* phase (256 DSPC and 64 Chol molecules). In this case, additionally, *ld* domains are simulated for different decreasing sizes. Following the procedure described above, the following *ld* patches have been generated: 192DOPC/320DSPC/80Chol (*ld*_192 domain), 128DOPC/384DSPC/96Chol (*ld*_128 domain), 96DOPC/416DSPC/104Chol (*ld*_96 domain) and 64DOPC/448DSPC/112Chol (*ld_64* domain). Simulations for the *lo* and *ld* nanodomains were run in the absence of any external electric field for at least 50 ns [21]. In both cases, equilibration is achieved in the first 10 ns, and during the remaining simulation time the phase-segregated nature of the simulated membrane systems is preserved (the simulation temperature is below the phase segregation temperature). Ten configurations corresponding to the last 10 ns of the latter simulations are saved as starting points to run the replicas for the simulations with an applied external electric field E. The electric field is applied in the direction normal to the membrane (x,y) plane, and each simulation is then run for a maximum of 20 ns or until membrane collapses due to an excessive pore size.

Structural analysis of the simulated membranes was performed by the use of Voronoi tessellation. The chosen key atoms for tessellation are the carbon group linking glycerol and phosphate groups for PC molecules, and the hydroxyl group for Chol molecules. Key atoms of each leaflet are projected onto a plane and Voronoi tessellation is performed (see [22] for details). Membrane properties like area per molecule, membrane thickness and lipid tail ordering can be computed and differential values can be assigned to each component of the membrane according to the corresponding Voronoi polygon. In particular, membrane thickness is computed for each PC molecule in the bilayer as the distance between its phosphorous group and the phosphorous group of the transbilayer PC neighbor molecule. All reported membrane properties for the simulations with an applied electric field are computed during the time period where the membrane keeps its bilayer conformation before any pore is generated.

3. Results and discussion

3.1. Raft-like patch membranes subjected to an electric field

3.1.1. Modification of membrane structural properties

An equilibration simulation of the central *lo* patch surrounded by a *ld* phase (raft-like membrane system) has been performed for 200 ns (no external electric field yet). After that time, the domain remains immiscible and the bilayer system keeps the heterogeneous distribution of its structural properties (see Fig. 1a). The area per PC molecule and membrane thickness have been averaged and plotted in Fig. 1b with respect to the distance to the center of mass of the raft-like domain, r. The values at the edges of the profiles are in agreement with the ones reported in Ref. [21] for homogeneous *lo* and *ld* membranes, and they are connected by a gradual variation along the domain boundary. As expected [6–10], when the electric field is applied, the total membrane

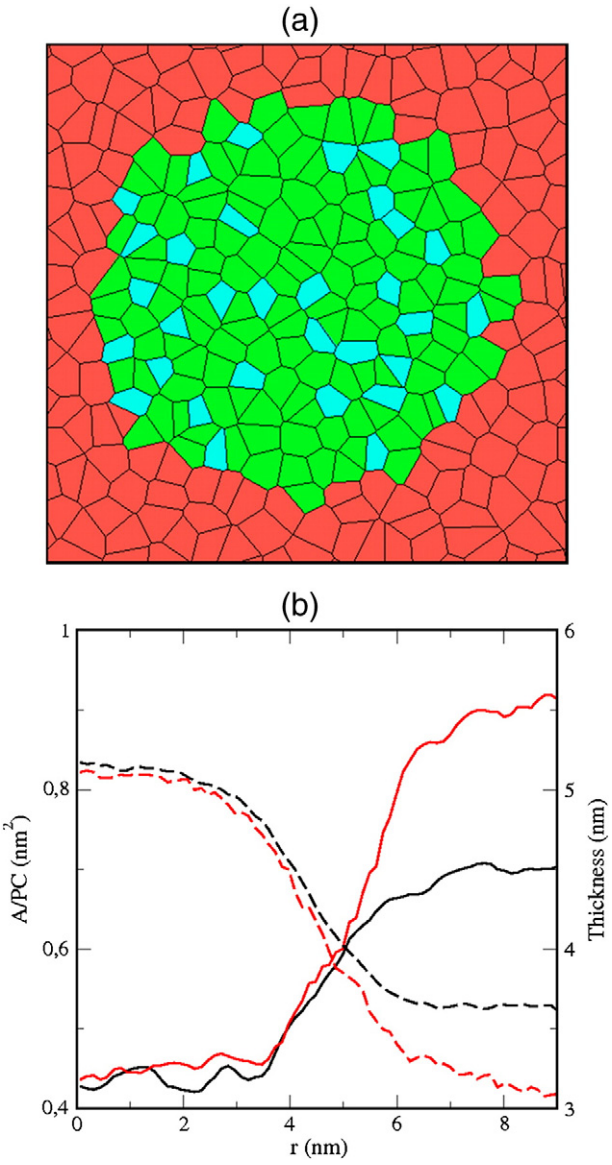

Fig. 1. Raft-like domain membrane. (a) Voronoi tessellation of a leaflet of the raft-like membrane systems after 200 ns of simulation ($E = 0$). Color code: DOPC (red), DSPC (green) and Chol (cyan). (b) Area per PC (solid) and thickness (dashed) profiles plotted with respect to the center of mass of the central patch. An average over the last 48 ns has been performed for the case $E = 0$ (black). For the simulation with an electric field (red, $E = 350$ mV/nm), the average over 10 ns has been performed before pore is generated.

area increases but it does with different contributions from its constituent phases. For the lowest electric field, $E = 350$ mV/nm [9], the changes in area per PC are computed before any pore is formed and plotted in Fig. 1b. Whereas the ordered domain only shows a slight increase of the area per DSPC (less than 2%), the disordered surroundings display a considerable expansion of area per DOPC (up to a 25% of increment). Consistently, membrane thickness is almost unaltered in the raft domain but significantly reduced (up to a 17%) in its surroundings (see Fig. 1b).

The internal ordering of lipids is also affected in a differential manner by the applied field. A typical way to quantify the internal ordering of lipid membranes is to compute the ordering of the phospholipid chains by means of the deuterium order parameter, S_{CD}, profiles [23]. The order parameter is defined as $S_{CD} = \langle \frac{3}{2}\cos^2\theta - \frac{1}{2} \rangle$ where θ is the angle between the carbon–deuterium bond and the bilayer normal, and the angular brackets denote averaging over time and over all bonds in a given carbon position. Larger values for $-S_{CD}$ imply higher chain ordering. A significant drop is typically found in the DOPC profiles at the location of its double bond due to its particular conformation. $-S_{CD}$ profiles are plotted in Fig. 2 for the DSPC molecules forming the core of the central patch ($r < 3$ nm, see Fig. 1b) and for the DOPC molecules in the disordered phase ($r > 6$ nm, see Fig. 1b). It is clear that the electric field has a stronger disordering effect in the *ld* phase than in the central *lo* domain. The average of the profiles, $<-S_{CD}>$, clearly quantifies this differential influence: $<-S_{CD}>$ is reduced in a 55% for DOPC molecules when applying the electric field (from 0.109 to 0.049), whereas the variation for DSPC is almost imperceptible (from 0.342 to 0.330).

Importantly for the electroporation process, insertion of water in the hydrophobic region of the membrane is significantly enhanced in the disordered phase and almost unaltered in the *lo* domain. In Fig. 3, the mass density "z"-profiles are plotted for the central patch ($r < 3$ nm, see Fig. 1b) and its disordered environment ($r > 6$ nm, see Fig. 1b). In the ordered domain, water hardly penetrates deeper than the location of phosphate groups, and the electric field does not modify this behavior (Fig. 3a). Instead, water molecules are promoted to explore more inner regions of the disordered membrane phase, particularly when the electric field is applied (Fig. 3b).

All changes in membrane properties reported so far can be related to a more general bilayer property: its cohesive nature, quantified by the area expansivity modulus that corresponds to the free energy variation relative to the variation of membrane area in the absence of bending and shear modes [24,25]. When an electric field is applied to a lipid bilayer, it induces a compressive stress perpendicular (and inward) to the bilayer surface that results in membrane expansion [24,26]. The response (expansion) of the membrane once the electric field is applied depends on the membrane expansivity modulus, so that it can be used to indirectly estimate its cohesive nature. Analysis of previous structural properties clearly shows that the electric field modifies significantly, and almost exclusively, the more disordered (less cohesive) regions of a heterogeneous lipid membrane. The ordered domain, instead, displays a much larger cohesion so it remains rather unaltered by the external electric field. It has been demonstrated experimentally that increasing membrane cohesion (for instance, by adding cholesterol) cohesion generally results in an electromechanical rupture of the membrane at larger critical voltages [25–27]. The differential cohesive nature of heterogeneous membranes is therefore going to be important in their electroporation behavior.

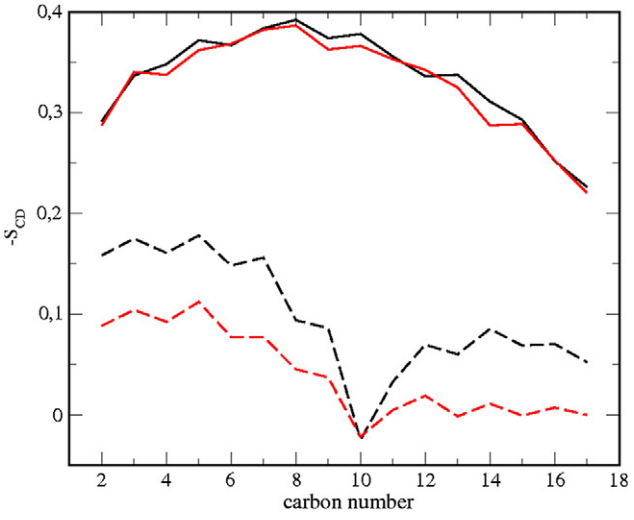

Fig. 2. Effects on lipid ordering. Deuterium order parameter $-S_{CD}$ profiles for DSPC molecules in the central *lo* patch (solid) and DOPC molecules in the surrounding *ld* phase (dashed). Profiles are plotted in the absence (black) and in the presence (red, $E = 350$ mV/nm) of an electric field. An average over 48 ns has been performed for the case $E = 0$ whereas for $E = 350$ mV/nm the average over 10 ns has been performed before pore is generated.

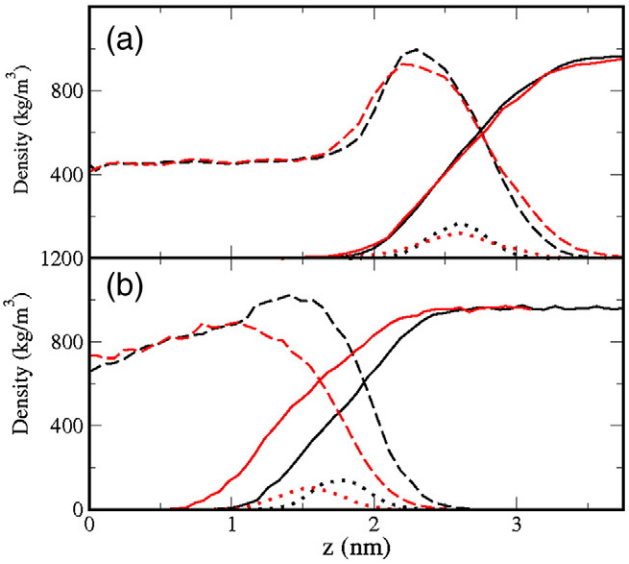

Fig. 3. Effects on water penetration. Density profiles for PC molecules (dashed), water (solid) and phosphate groups (dotted) are plotted in the absence (black) and in the presence (red, $E = 350$ mV/nm) of an electric field. (a) Central *lo* patch. (b) Surrounding *ld* phase. An average over 48 ns has been performed for the case $E = 0$, whereas for $E = 350$ mV/nm the average over 10 ns has been performed before pore is generated.

3.1.2. Electroporation of raft-like membranes

The simulations performed for heterogeneous raft-like patched membranes also display the generation of stable water pores. As it is shown in Fig. 4, the sequence of pore formation follows the mechanism reported in previous studies [6–10]. In short, the applied external field disorders the water–membrane interface and generates a water defect (fluctuation) that initiates pore formation. The water defect develops into a column of water molecules that penetrates into the inner region of the bilayer, forming a non-stable hydrophobic pore. Further on, phospholipid head groups reorient in order to cover the water column and form a stable hydrophilic pore. Interestingly, Fig. 4 shows how the poration process takes place exclusively in the disordered DOPC phase of the membrane (see below). For completeness, it is important to notice that the electropores generated in the simulations grow continuously during the time the electric field is applied. Under these circumstances the pore expands to the size of the simulated bilayer patch and the membrane collapses. Reversible pores can be obtained if the electric field is removed [10], or stable pores can be obtained and maintained with a fixed size by reducing the applied field [28].

Different electric field values and 10 replicas of the equilibrated raft-like membrane for each value have been simulated. The poration times τ (time period before pore formation is initiated upon the electric field is applied) are provided in Table 1, and reveal the stochastic nature of

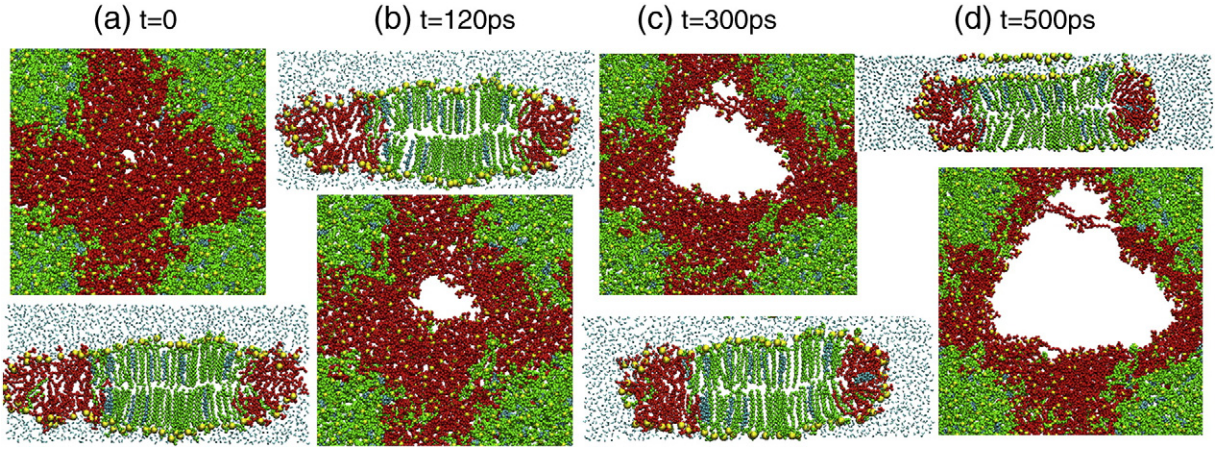

Fig. 4. Electroporation of a raft-like membrane. Snapshots for the pore formation and growth processes in the raft-like domain membrane system with an applied electric field $E = 350$ mV/nm. The stages of pore initiation (panels a), stabilization (panels b) and growth (panels c and d) are plotted. At each time, two views are presented: a surface (x,y) view, and a 0.3 nm-thick slice view in one diagonal direction (from the left-upper corner to the right-bottom corner). In the surface views periodic boundary conditions have been used to place the pore at the center of the panels. DOPC, DSPC and Chol molecules are plotted in red, green and cyan, respectively. Phosphate groups of PC molecules are plotted using yellow beads. Water molecules are plotted with blue sticks. For clarity, water molecules are removed in the (x,y) view.

the electroporation phenomenon. The occurrence of water fluctuations in the water/membrane interface increases with the applied field, so if a stronger field is applied, a shorter time is needed to porate the membrane [9]. More importantly, however, is the following observation: in all simulations, pores are formed in the disordered region of the membrane system. In the 60 simulations of the raft-like domain, the pore (as it is shown in Fig. 4) is always initiated and grows in the disordered lipid phase, so that lipids in the ordered phase (DSPC and Chol) are not involved in pore formation and stabilization until it has extended over most of the membrane surface.

Table 1
Poration time τ (ns) for 10 simulation replicas of each structured membrane system at different electric fields[a,b].

E (mV/nm)	Raft-like domain									
350	12.2	5.2	7.9	17.0	11.5	8.6	3.3	7.5	4.8	3.9
400	3.9	1.1	2.1	4.7	2.6	6.1	0.7	3.8	4.5	3.7
500	1.7	2.3	<0.5	4.3	3.0	1.8	1.8	5.1	2.0	<0.5
750	<0.5	1.5	<0.5	1.8	3.6	0.8	2.1	<0.5	<0.5	<0.5
1000	<0.5	<0.5	<0.5	<0.5	<0.5	<0.5	<0.5	<0.5	<0.5	<0.5
1500	<0.5	<0.5	<0.5	1.2	<0.5	<0.5	<0.5	<0.5	<0.5	<0.5
	ld_256 domain									
350	17.2	4.7	9.6	11.1	7.0	2.9	6.8	6.6	13.3	8.2
400	0.8	1.0	3.8	4.0	3.5	1.5	2.2	8.7	4.7	5.8
500	3.8	<0.5	<0.5	0.6	0.8	3.0	2.7	1.1	4.1	<0.5
750	<0.5	<0.5	<0.5	1.2	1.2	<0.5	<0.5	3.0	2.7	<0.5
1000	1.3	<0.5	<0.5	<0.5	<0.5	<0.5	<0.5	<0.5	<0.5	<0.5
1500	<0.5	<0.5	<0.5	<0.5	<0.5	<0.5	<0.5	<0.5	<0.5	<0.5
	ld_192 domain									
350	18.7	10.1	4.2	3.2	8.6	1.8	2.7	12.0	5.9	9.8
	ld_128 domain									
350	7.5	12.0	2.7	1.5	8.5	<0.5	5.5	4.3	2.2	6.3
	ld_96 domain									
350	1.8	3.2	<0.5	5.2	6.5	3.9	3.2	2.8	5.4	<0.5
	ld_64 domain									
350	3.4	2.0	<0.5	<0.5	1.7	<0.5	<0.5	4.0	2.3	1.1
400	<0.5	<0.5	3.2	1.2	<0.5	<0.5	<0.5	1.5	<0.5	<0.5
500	<0.5	<0.5	<0.5	<0.5	<0.5	<0.5	2.1	<0.5	<0.5	<0.5
750	<0.5	<0.5	<0.5	<0.5	<0.5	<0.5	<0.5	<0.5	<0.5	<0.5
1000	<0.5	<0.5	<0.5	<0.5	<0.5	<0.5	<0.5	<0.5	<0.5	<0.5
1500	<0.5	<0.5	<0.5	<0.5	<0.5	<0.5	<0.5	<0.5	<0.5	<0.5

[a]Pore formation causes a sudden increase of the total membrane area that it is used here to determine the poration time τ.
[b]<0.5 means that the pore is generated right after the electric field is applied.

3.2. Liquid-disordered domain membranes subjected to an electric field

3.2.1. Electroporation of ld domain membranes

Electroporation of the *ld*_256 domain, that corresponds to the inverse configuration than the raft-like membrane, has been attempted and similar results are obtained. First, the electric field perturbs almost exclusively the properties of the disordered region (complementary profiles to those shown in Fig. 1b are obtained). Second, 10 replicas of the membrane systems have been simulated at different values of the electric field, and in all cases electropores are formed in the *ld* phase. Poration times are provided in Table 1, showing a similar behavior than for the raft-like membrane analyzed above.

Other initial configurations for coexisting *lo*/*ld* membrane systems have been attempted, and the exclusive generation of pores in the *ld* regions reported above is reproduced in all cases. An extreme and interesting situation is that of a very small *ld* central patch of 64 DOPC molecules surrounded by a *lo* phase consisting in 448 DSPC and 112 Chol molecules (*ld*_64 domain, see Fig. 5a). Again, the electric field mainly affects to the properties of the disordered phase (see Fig. 5b for the area per molecule and membrane thickness) before the electropore is generated. Ten simulation replicas have been performed at different values for the electric field, and the corresponding poration times are provided in Table 1.

Despite its reduced surface, electropores are formed in the small *ld* region of the membrane for the 60 simulated membranes. A typical sequence of the electroporation process has been detailed in Fig. 6. It has to be noticed that, as a general behavior, only DOPC molecules are involved in pore initiation and in the initial stages of hydrophilic pore construction. This observation is quantified in Fig. 7 where the tilt angle distribution for PC species is plotted for the first nanosecond after pore initiation. The tilt angle is taken as the angle between the z-axis (bilayer normal) and the vector connecting the phosphorous atom group and the last carbon group of each acyl chain. Fig. 7 clearly shows that once the pore is formed, most DOPC molecules are already rotated in order to protect and stabilize the hydrophilic pore, whereas almost all DSPC lipids still preserve their 'vertical' orientation. As long as the pore grows, the ordered region of the membrane becomes finally affected, and some DSPC and Chol molecules also reorient to protect the pore from water molecules.

Electroporation of such small domains also reveals two aspects that deserve particular attention. First, visual inspection of the electroporation

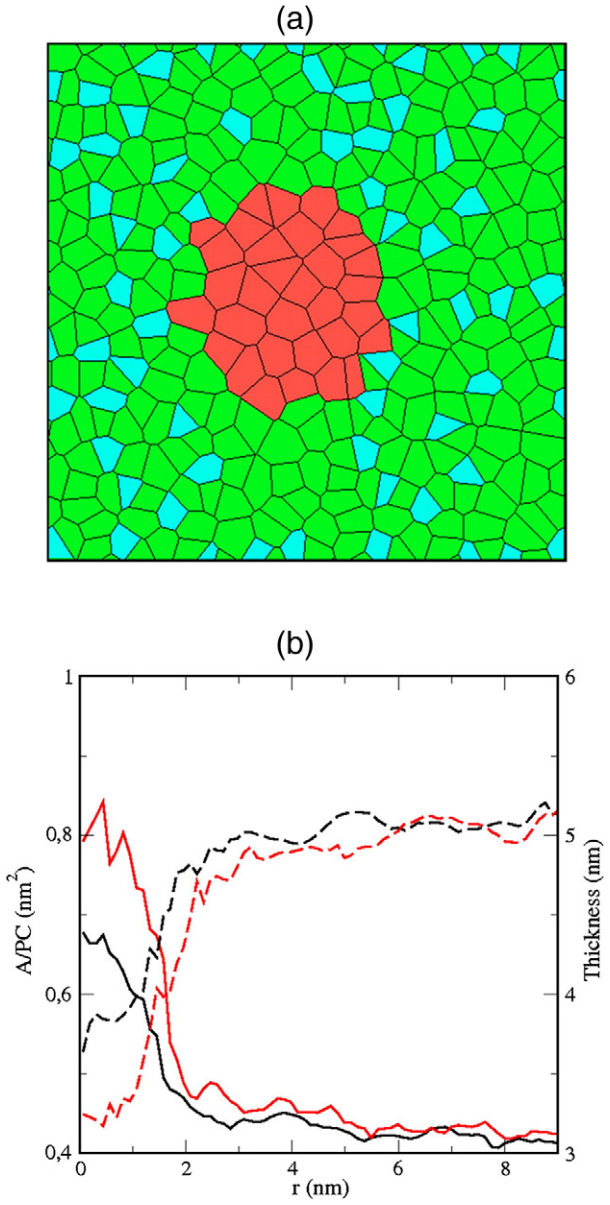

Fig. 5. Small *ld*_64 domain membrane. (a) Voronoi tessellation of a leaflet of the small *ld*_64 domain membrane systems after 100 ns of simulation ($E = 0$). Color code: DOPC (red), DSPC (green) and Chol (cyan). Bottom panels: area per PC (solid) and thickness (dashed) profiles plotted with respect to the center of mass of the central patch. An average over the last 48 ns has been performed for the case $E = 0$ (black). For the simulation with an electric field (red, $E = 350$ mV/nm), the average over 3 ns has been performed before pore is generated.

process indicates that pores are initiated in the middle of the small disordered lateral domains. Second, intriguingly, poration times of the small *ld*_64 domain are much shorter than those for the raft-like and its complementary *ld*_256 domain membrane systems analyzed above. Both aspects are analyzed in the following subsections.

3.2.2. Domain boundaries are not electroporated

An important aspect needs to be considered before conjecturing about the electroporation of structured membranes containing regions with different lipid ordering: the existence of an ordered/disordered interface. The role of lateral domain boundaries is fundamental in another mechanism for pore formation observed in membranes at the phase transition point. Spontaneous ion permeability, measured as quantized conductance events, was reported a few decades ago in simple bilayers at a temperature close to the melting transition [29–31]. The physical origin of this ionic conductance is the spontaneous formation of pores due to thermal membrane area fluctuations. Area fluctuations are more likely when the membrane is close to its transition temperature: the work needed to create a pore is proportional to its lateral compressibility, that in turn is proportional to the excess heat capacity [32,33]. At the melting transition, heat capacity reaches a maximum, so permeability by means of transient membrane fluctuations is enhanced.

Interestingly, the latter mechanism for pore formation has been found to take place more likely in the boundaries between the emerging lipid domains since they display the largest area fluctuations. At the transition, domain interfaces reach a maximum and permeability is then significantly enhanced. Consistently, permeability has been proved to be proportional to the length of domain boundaries by Monte Carlo simulations [34,35].

The simulations performed here correspond to another mechanism for membrane permeability based on the application of high electric fields: electroporation. In this case, the applied field besides reducing the cohesive nature of the bilayer (namely, its area expansivity modulus), it also strongly disorders the water/membrane interface and generates water fluctuations. These fluctuations correspond to groups of a few water molecules that temporary penetrate the membrane. Water fluctuations may either evolve until the full pore is formed or retract after some time, recovering the initial configuration. This process has been well described at the molecular level by means of molecular dynamics simulations [6–10].

The two mechanisms mentioned so far display completely different characteristics. Thermodynamically driven pores are formed when the membrane lipid mixture is close to the main gel-liquid transition (melting transition). Membrane fluctuations are responsible for pore formation, and their characteristic time scale is of the order of tens of milliseconds [29–33], so the study of this poration mechanism is unavailable by means of atomistic molecular dynamics simulations. On the other hand, electroporation is forced by applying strong electric fields. Water fluctuations are then responsible for the initiation of pore formation and the presence of membrane fluctuations is not required. The characteristic time scale of this mechanism ranges from nanoseconds to microseconds [1–10].

The high occurrence of pore formation in lipid–lipid interfaces found when the membrane is close to a phase transition deserves also particular attention in the electroporation context. Actually, even far from the transition point (as it is the case in the presented simulations), domain boundaries contribute with a line tension energy penalty and may act as membrane 'defects'. Consequently, the formation of a pore could be expected to be energetically less unfavorable in the domain boundary than in a homogeneous region of strongly phase-segregated membranes. Visual inspection of the performed simulations, however, discards this possibility for the electroporation mechanism: electropores are initiated in random locations of the disordered regions without any preference for the domain boundary. Simulations clearly show that lipid domain boundaries are not electroporated, contrarily with what happens in the thermodynamic pore formation mechanism. As an example, Fig. 8 shows a snapshot for each *lo*_256 domain replica at an early stage of pore initiation. Even for the case of the *ld*_64 domain, boundaries are not electroporated: in the 60 simulated replicas of this membrane system, pores are initiated in the very middle of the small disordered domain.

3.2.3. Smaller domains become electroporated sooner

Although the area of the *ld*_64 domain is about four times smaller than the area of the *ld*_256 domain, its average poration time $\langle\tau\rangle$ is more than five times shorter. This size effect is investigated in more detail by performing the simulations with different domain sizes (*ld*_96, *ld*_128, *ld*_192 domains) at the same electric field $E = 350$ mV/nm. Ten replicas for each domain size have been performed and the corresponding poration times are provided in Table 1.

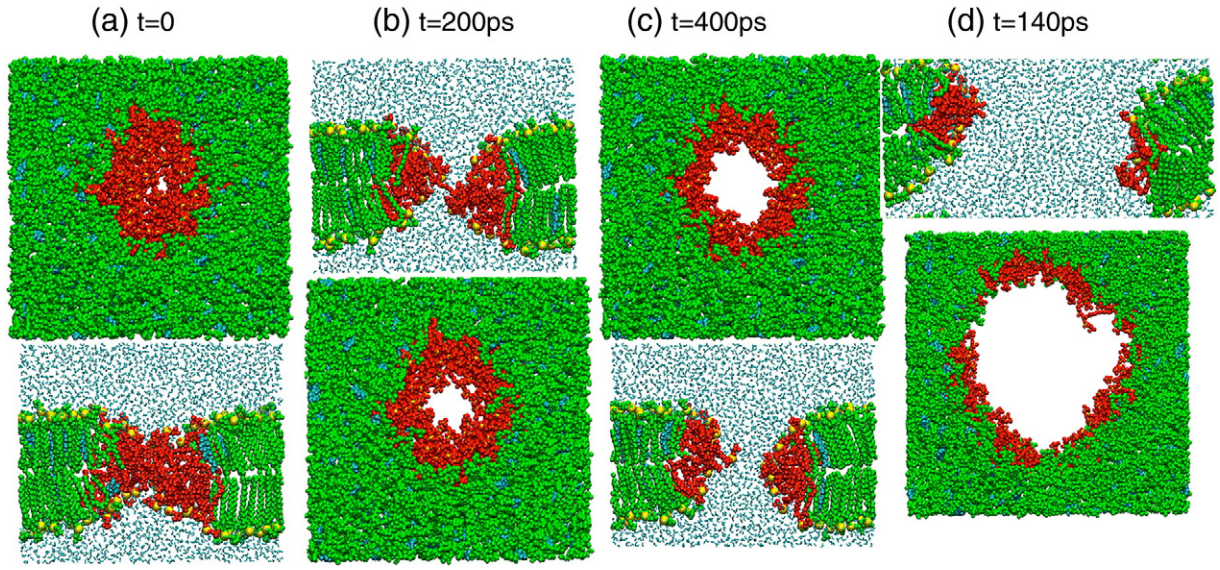

Fig. 6. Electroporation of the small *ld*_64 domain membrane. Snapshots for the pore formation and growth processes in the small *ld*_64 domain membrane system with an applied electric field $E = 350$ mV/nm. The stages of pore initiation (panels a), stabilization (panels b) and growth (panels c and d) are plotted. At each time, two views are presented: a surface (x,y) view, and a 0.3 nm-thick slice (x,z) view in the y-axis direction traversing the middle of the simulated system. The same color in Fig. 4 code is used. For clarity, water molecules are removed in the (x,y) view.

The averaged poration times, $\langle\tau\rangle$, show a clear dependence with domain size: $\langle\tau\rangle = 1.7 \pm 0.6$ ns for the *ld*_64 domain, 3.3 ± 1.0 ns for the *ld*_96 domain, 5.1 ± 1.7 ns for the *ld*_128 domain, 7.7 ± 2.5 ns for the *ld*_192 domain, 8.7 ± 2.0 ns for the *ld*_256 domain, and 8.2 ± 2.0 ns for the raft-like domain (see Fig. 9). Despite the small sample of simulations and the large standard deviations, the results presented in Fig. 9 reveal a clear and consistent domain size effect in the electroporation times, and show that smaller disordered patches are faster to porate (at least at the nanometric scale used in the simulations and in the context of high electroporation voltages).

The physical mechanism that explains the unexpectedly short poration times for the small *ld* patch bilayers can be understood by looking at the particular arrangement of water molecules close to the membrane/water interface (see Fig. 10). Notice that two 'cones' of water molecules are formed at the interface with the small *ld*_64 patch at both sides of the membrane, even in the absence of any electric field. These water 'cones' are perfect precursors of pore-initiating water fluctuations. As stated in the previous section, a water fluctuation requires that a group of a few water molecules got transiently 'disconnected' from the bulk in order to penetrate the membrane. This is more likely to happen at the tip of the cone-like configuration than in a planar arrangement of molecules. One of these fluctuations may eventually traverse the membrane once the electric field is applied, so that electropore initiation is targeted to the disordered lipid region. The observed systematic occurrence of the initial stages of pore formation in the very center of the *ld*_64 domain also supports the latter argument.

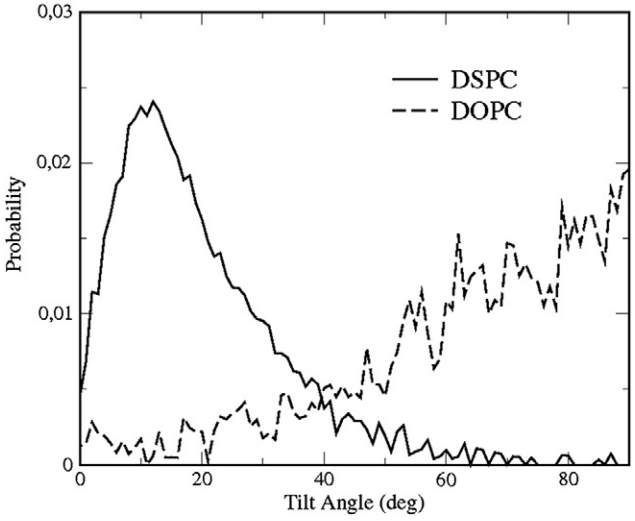

Fig. 7. Differential tilt distribution during electroporation. Distribution of tilt angles for the DSPC and DOPC molecules in the small *ld*_64 patch membrane once the hydrophilic electropore is already formed ($E = 350$ mV/nm). Average over 1 ns has been performed.

3.3. Conclusions

It is well accepted that the preferential packing of cholesterol and saturated lipids to form a liquid-ordered phase, segregated from a liquid-disordered medium rich in unsaturated lipids, underlies lipid lateral heterogeneity in cell membranes. Consequently, a realistic description of the electroporation mechanism in cell membranes by means of MD simulations of lipid membranes must account for the presence of segregated *lo* and *ld* phases.

The systematic set of simulations of structured lipid bilayers presented here demonstrates that an applied electric field mainly perturbs the more disordered lipid phases, since they display a less cohesive nature than phases with a higher lipid ordering. The analysis of the electrically induced modifications of area per lipid, bilayer thickness, chain ordering and density profiles at different phases of heterogeneous membranes supports this conclusion. Importantly, and as a main consequence of the latter, the generation of electropores is systematically observed to take place in the disordered regions of the membrane.

The fact that disordered membranes become electroporated at lower electric potentials than ordered bilayers was proven by molecular dynamics simulations [9] and may anticipate some of the results reported in this paper. However, there is an important element that should be considered in the study of the electroporation of structured membranes: the existence of an ordered/disordered interface. Domain boundaries between lipid lateral domains contribute with a line tension energy penalty and may act as membrane 'defects'. Consequently, the formation of a pore could be expected to be energetically less unfavorable in the domain boundary than in a homogeneous region of the membrane. Actually, in the context of thermodynamically driven

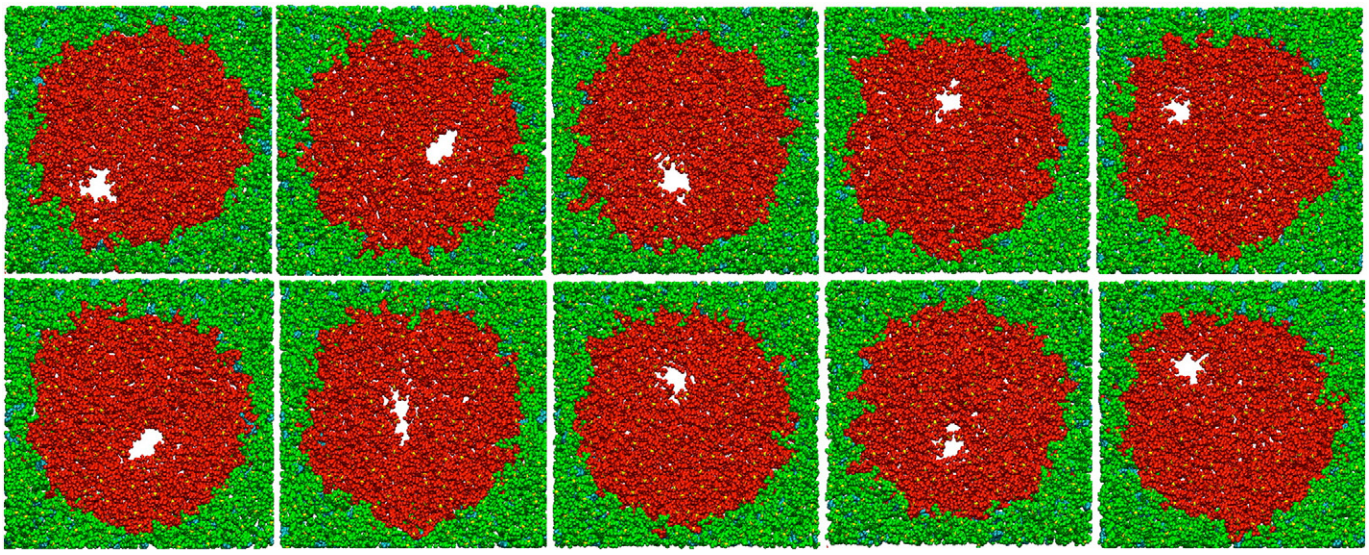

Fig. 8. Domain boundaries are not electroporated. Snapshots corresponding to the initial stages of pore formation for each one of the 10 replicas of the *ld*_256 domain ($E = 350$ mV/nm). A surface (x,y) view is provided. The same color in Fig. 4 code is used. For clarity, water molecules are removed.

pore formation (lipid bilayers close to a lipid phase transition), the likelihood of finding a membrane pore is found to be maximum at domain boundaries. The observations from the performed simulations, however, discard this possibility for the electroporation mechanism: electropores are initiated in random locations of the disordered regions without any preference for the domain boundary.

At this point it is important to notice that the reported preference for disordered regions does not mean that ordered phases cannot be electroporated. Actually, there is a large experimental evidence of electroporation of liquid-ordered and gel membrane phases, and molecular dynamics also provide some examples [9]. The precise conclusion that has to be extracted from the reported simulations is that in the context of electroporation (high voltages) of membranes displaying *lo*/*ld* coexistence, the disordered regions are porated much sooner than the ordered ones, and this could be relevant in the context of electroporation techniques using short pulses at the nanosecond scale. In this situation, the disordered regions of the membrane are more likely to be porated than the ordered ones.

The simulations also show a dependence of the electroporation times with the size of the disordered domains. Interestingly, smaller *ld* domains display shorter electroporation times and this observation has been justified by the cone-like arrangement of adjacent water molecules. According to the obtained electroporation times, this finding could be also relevant for electroporation techniques using high electric fields and very short pulses (in the scale of few nanoseconds) that have recently generated intense interest for their use in cancer treatments [36].

The findings reported in this paper indicate that the induction of electropores *in vivo* does not happen randomly on the cell membrane surface but preferentially on its smaller and more disordered lateral domains, so that electro-induced pore-mediated transport processes may locally affect specific regions of the cell. This conclusion may have a relevant significance in the experimental application of cell electroporation *in vivo*.

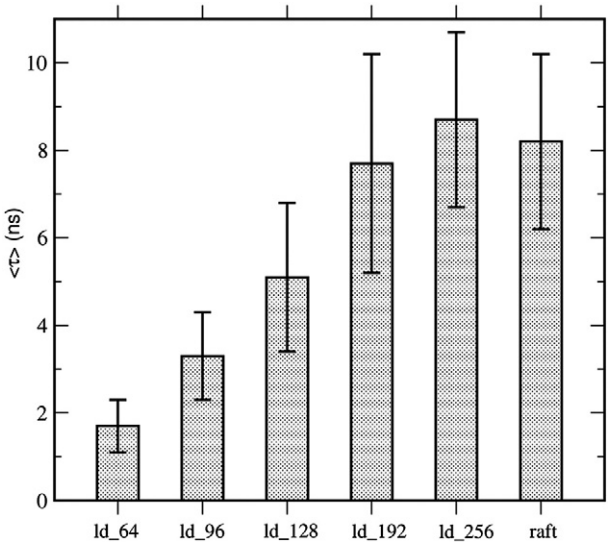

Fig. 9. Smaller domains are easier to electroporate. Average of the electroporation times (over 10 replicas for each system) for the different structured membranes simulated in this paper. Errors bars correspond to the standard deviation.

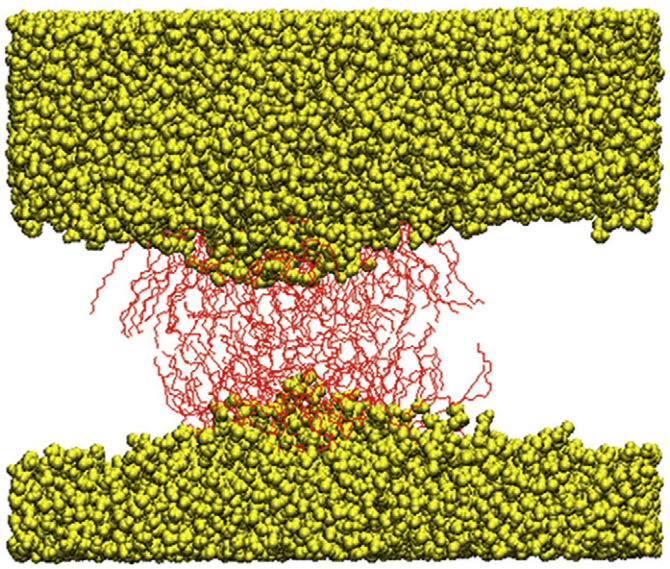

Fig. 10. Poration is targeted to the *ld*_64 domain by a water cone. Cone-like arrangement of water molecules (yellow beads) after 100 ns of equilibration of the small *ld*_64 patch membrane system (no external electric field). DOPC molecules forming the *ld* domain are plotted using red sticks.

Finally, it is important to notice that the limitations of the standard all-atom MD technique determine the context of applicability of the reported results and conclusions. First, all-atom MD simulations are restricted to simulation times of a few hundred of nanoseconds, much shorter than the typical thermodynamically driven poration times in the scale of milliseconds. Even the use of coarse-grained MD simulations is far from the millisecond's challenge (e.g. MARTINI [37] simulations of relatively large membrane patches reach several microseconds). Another important drawback of standard MD simulations is the control of the pH of the membrane solution. pH is recognizably one important factor that affects membrane behavior and stability. For example, the melting temperature of a lipid membrane depends on pH [38]. In the context of electroporation, pH at the aqueous environment nearby the membrane can be altered by the presence of external electric fields and this, in turn, may affect both the charge distributions at the membrane/water interface and the thermodynamic stability of the lipid mixture [39]. However, despite its undeniable importance, pH is usually ignored in molecular dynamics due to its high complexity in terms of modeling. To overcome this problem, constant-pH MD methodologies where the pH is a control parameter of the simulation are being developed [40,41]. In these approaches the protonation states of ionizable groups are allowed to change dynamically during the MD simulation, and are obtained from a combination of continuum electrostatics calculations and a Monte Carlo simulation of protonation equilibrium. These methods have been successfully applied to proteins (see for example [42]) but little work has been published so far for lipid bilayers (see [43] for simulations of fatty acids aggregates using the MARTINI force field). Concluding, the presented simulations and the corresponding conclusions are valid in the context electroporation (high voltages/fast pore formation) of phase-segregated *lo*/*ld* lipid membranes (far from the segregation transition) at a fixed pH where the zwiterionic lipid molecules are neutral. The study of poration phenomena in the proximity to a phase transition and/or the influence of pH on the poration process are beyond the scope of this work.

Acknowledgment

Financial support has been provided by SEID through project BFU2010-21847-C02-02 and by DURSI through project 2009-SGR-1055.

References

[1] T.Y. Tsong, Electroporation of cell membranes, Biophys. J. 60 (1991) 297–306.
[2] L. Mir, M.F. Bureau, J. Gehl, R. Rangara, D. Rouy, J.-M. Caillaud, P. Delaere, D. Branellec, B. Schwartz, D. Scherman, High-efficiency gene transfer into skeletal muscle mediated by electric pulses, Proc. Natl. Acad. Sci. U. S. A. 96 (1999) 4262–4267.
[3] T.Y. Tsong, Electric modification of membrane permeability for drug loading into living cells, Methods Enzymol. 149 (1987) 248–259.
[4] LL.M. Mir, S. Orlowski, The basis of electrochemotherapy in electrochemotherapy, electrogenetherapy and transdermal drug delivery: electrically mediated delivery of molecules to cells, Springer, 2000.
[5] M. Belehradek, C. Domenge, B. Luboinski, S. Orlowski, J. Belehradek, LL.M. Mir, Electrochemotherapy, a new antitumor treatment. First clinical phase I–II trial, Cancer 72 (1993) 3694–3700.
[6] D.P. Tieleman, The molecular basis of electroporation, BMC Biochem. 5 (2004) 10.
[7] M. Tarek, Membrane electroporation: a molecular dynamics study, Biophys. J. 88 (2005) 4045–4053.
[8] M.J. Ziegler, P.T. Vernier, Interface water dynamics and porating electric fields for phospholipid bilayers, J. Phys. Chem. B 112 (2008) 13588–13596.
[9] M.L. Fernández, G. Marshall, F. Sagués, R. Reigada, Structural and kinetic molecular dynamics study of electroporation in cholesterol-containing bilayers, J. Phys. Chem. B 114 (2010) 6855–6865.
[10] Z.A. Levine, P.T. Vernier, Life cycle of an electropore: field-dependent and field-independent steps in pore creation and annihilation, J. Membr. Biol. 236 (2010) 27–36.
[11] M. Breton, L. Delemotte, A. Silve, LL.M. Mir, M. Tarek, Transport of siRNA through lipid membranes driven by nanosecond electric pulses: an experimental and computational study, J. Am. Chem. Soc. 134 (2012) 13938–13941.
[12] G. Vereb, J. Szöllösi, J. Matkó, P. Nagy, T. Farkas, L. Vigh, L. Mátyus, T. Waldmann, A.S. Damjanovich, Dynamic, yet structured: the cell membrane three decades after the Singer–Nicolson model, Proc. Natl. Acad. Sci. U. S. A. 100 (2003) 8053–8058.
[13] S.L. Veatch, S.L. Keller, Miscibility phase diagrams of giant vesicles containing sphingomyelin, Phys. Rev. Lett. 94 (2005) 148101.
[14] J.R. Silvius, Role of cholesterol in lipid raft formation: lessons from lipid model systems, Biochim. Biophys. Acta 1610 (2003) 174–183.
[15] K. Simons, E. Ikonen, Functional rafts in cell membranes, Nature 387 (1997) 569–572.
[16] E. Lindahl, B. Hess, D. van der Spoel, GROMACS 3.0: a package for molecular simulation and trajectory analysis, J. Mol. Model. 7 (2001) 306–317.
[17] O. Berger, O. Edholm, F. Jahnig, Molecular dynamics simulations of a fluid bilayer of dipalmitoylphosphatidylcholine at full hydration, constant pressure, and constant temperature, Biophys. J. 72 (1997) 2002–2013.
[18] H. Martinez-Seara, T. Róg, M. Karttunen, R. Reigada, I. Vattulainen, Influence of *cis* double-bond parameterization on lipid membrane properties: how seemingly insignificant details in force-field change even qualitative trends, J. Chem. Phys. 129 (2008) 105103.
[19] M. Holtje, T. Forster, B. Brandt, T. Engels, W. von Rybinski, H.-D. Holtje, Molecular dynamics simulations of stratum corneum lipid models: fatty acids and cholesterol, Biochim. Biophys. Acta 1511 (2001) 156–167.
[20] H. Martinez-Seara, T. Róg, M. Karttunen, I. Vattulainen, R. Reigada, Cholesterol induces specific and orientational order in cholesterol/phospholipid membranes, PLoS One 5 (2010) e11162.
[21] R. Reigada, Atomistic study of lipid membranes containing chloroform: looking for a lipid-mediated mechanism of anesthesia, PLoS One 8 (2013) e52631.
[22] S.A. Pandit, S. Vasudevan, S.W. Chiu, R.J. Mashl, E. Jakobsson, et al., Sphingomyelin-cholesterol domains in phospholipid membranes: atomistic simulation, Biophys. J. 87 (2004) 1092–1100.
[23] J.H. Davis, The description of membrane lipid conformation, order and dynamics by ^{2}H-NMR, Biochim. Biophys. Acta 737 (1983) 117–171.
[24] J.M. Crowley, Electrical breakdown of bimolecular lipid membranes as an electromechanical instability, Biophys. J. 13 (1973) 711–724.
[25] E. Evans, D. Needham, Physical properties of surfactant bilayer membranes: thermal transitions, elasticity, rigidity, cohesion and colloidal interactions, J. Phys. Chem. 91 (1987) 4219–4228.
[26] D. Needham, R.M. Hochmuth, Electro-mechanical permeabilization of lipid vesicles. Role of membrane tension and compressibility, Biophys. J. 55 (1989) 1001–1009.
[27] S. Koronkiewicz, S. Kalinowski, Influence of cholesterol on electroporation of bilayer lipid membranes: chronopotentiometric studies, Biochim. Biophys. Acta 1661 (2004) 196–203.
[28] M.L. Fernández, G. Marshall, F. Sagués, R. Reigada, Size-controlled nanopores in lipid membranes with stabilizing electric fields, Biochem. Biophys. Res. Commun. 423 (2012) 325–330.
[29] D. Papahadjopoulos, K. Jacobson, S. Nir, T. Isac, Phase transitions in phospholipid vesicles, fluorescence polarization and permeability measurements concerning the effect of temperature and cholesterol, Biochim. Biophys. Acta 423 (1973) 330–340.
[30] J.F. Nagle, H.L. Scott, Lateral compressibility of lipid mono and bilayers: theory of membrane permeability, Biochim. Biophys. Acta 513 (1978) 236–243.
[31] V.F. Antonov, V.V. Petrov, A.A. Molnar, D.A. Predvoditelev, A.S. Ivanov, The appearance of single ion channels in unmodified lipid bilayer membrane at the phase transition temperature, Nature 283 (1980) 585–588.
[32] T. Heimburg, Lipid ion channels, Biophys. Chem. 150 (2010) 2–22.
[33] B. Wunderlich, C. Leirer, A.-L. Idzko, U.F. Keyser, A. Wixforth, V.M. Myles, T. Heimburg, M.F. Schneider, Phase-state dependent current fluctuations in pure lipid membranes, Biophys. J. 96 (2009) 4592–4597.
[34] L. Cruzeiro-Hansson, O.G. Mouritsen, Passive ion permeability of lipid membranes modeled via lipid-domain interfacial area, Biochim. Biophys. Acta 944 (1988) 63–72.
[35] E. Corvera, O.G. Mouritsen, M.A. Singer, M. Zuckermann, The permeability and the effect of acyl-chain length for phospholipid bilayers containing cholesterol: theory and experiment, Biochim. Biophys. Acta 1107 (1992) 261–270.
[36] M. Breton, LL.M. Mir, Microsecond and nanosecond electric pulses in cancer treatments, Bioelectromagnetics 33 (2012) 106–123.
[37] S.J. Marrink, H.J. Risselada, S. Yefimov, D.P. Tieleman, A.H. de Vries, The MARTINI force field: coarse grained model for biomolecular simulations, J. Phys. Chem. B 111 (2007) 7812–7824.
[38] H. Träuble, H. Eibl, Electrostatic effects on lipid phase transitions: membrane structure and ionic environment, Proc. Natl. Acad. Sci. U. S. A. 71 (1974) 214–219.
[39] H. Träuble, Membrane electrostatics, in: S. Abrahamsson, I. Pascher (Eds.), The Structure of Biological Membranes, Plenum Press, NY, 1977, pp. 509–550.
[40] A.M. Baptista, V.H. Teixeira, C.M. Soares, Constant-pH molecular dynamics using stochastic titration, J. Chem. Phys. 117 (2002) 4184–4200.
[41] M. Machuqueiro, A.M. Baptista, Constant-pH molecular dynamics with ionic strength effects: protonation-conformation coupling in decalysine, J. Phys. Chem. B 110 (2006) 2927–2933.
[42] J.A. Wallace, J.K. Shen, Predicting pKa values with continuous constant pH molecular dynamics, Methods in Enzymology, vol. 466, Elsevier, 2009, (Chapter 19).
[43] W.F. Drew Bennett, A.W. Chen, S. Donnini, G. Groenhof, D.P. Tieleman, Constant pH simulations with the coarse-grained MARTINI model – Application to oleic acid aggregates, Can. J. Chem. 91 (2013) 839–846.